Effects of gaseous pyrolysis products on aluminium recycling yield

[1]Jaroni, B.; [1]Gisbertz, K.; [2]Rombach, G.; [1]Friedrich, B.

[1]RWTH Aachen University, IME Process Metallurgy and Metals Recycling, Aachen, Germany
[2]Hydro Aluminium Rolled Products GmbH, Bonn, Germany

After a coated aluminum product has reached the end of life cycle it needs to be recycled in an economical, effective and ecological way. State-of-the-art is the thermal removal of coatings and other organic fractions via treatment by pyrolysis prior to melting. In modern twin chamber furnaces this step takes place inside the scrap melting chamber. Through different construction methods, it is possible to use the gaseous pyrolysis products for an internal combustion in order to safe natural gas. Lab-scale experiments have shown that the average residence time is too short to complete the pyrolysis. It has to be considered that the pyrolysis continuous while the scrap block is pushed under the aluminum melt. By reason of this production procedure, gaseous reaction products, e.g. CO, CO_2 and C_xH_y, have a long contact time inside the melt. It is assumed that the dross formation increases rapidly as a result of various gas-melt reactions. Based on this assumption the aim of this work is the evaluation of the influence of gaseous pyrolysis reaction products on the dross formation by the simulation in lab-scale experiments. Therefore, typical pyrolysis gases are injected into the melt via a gas purging device. Furthermore, the magnesium content of the aluminum melt is varied to show its impact in addition to the gases.

1 Introduction

The pyrolytic process in chamber furnaces is located on the bridge inside the scrap melting chamber. In modern twin chamber furnaces the average charging time is 25 minutes. The time interval depends on bath temperature, bath level, atmosphere composition and security door lock time. This time interval simultaneously limits the duration of scrap heating, organic scission and combustion of carbon released from the scrap surface. With the next scrap charge the de-coated scrap is pushed into the aluminum melt which means that charging time is equal to the duration of the thermal pretreatment. The industrial de-coating time seems to be too short for a complete pyrolysis step especially inside compacted scrap, e.g. coil-leftovers and packages. The de-coating grade is a function of time, temperature, heat transfer and package density. In comparison with aluminum blocks the heat transfer of scrap packages is reduced. As a result of the package structure the pyrolysis products cannot leave the compacted material with a typical density is well below 2 g/cm^3.

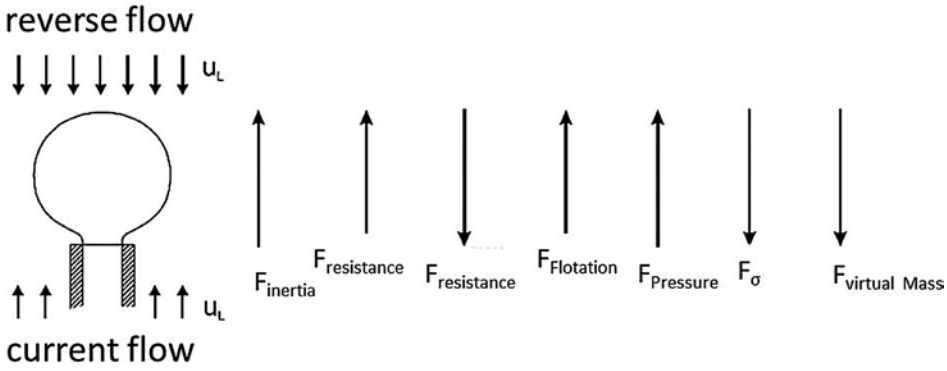

Fig. 1: Balance of forces

2 Gas-liquid reactions

The reaction between gaseous reaction products and liquid aluminum follows a certain pattern. The bubble formation depends on the porosity of the medium. In the case of a scrap package there is a high variation of the hole diameter. Generally speaking, the bubble diameter is a function of surface tension, the pore diameter and the amount of formed gas. With a porous medium as gas distributor only the larges pores are outgassing at low gas flow rates. An increasing gas flow rate also enables the gas evolution on/at/of smaller openings, so that the gas flow is distributed more on the entire surface of the porous medium. The most common example of viewing bubble formation as a result of the bubble size goes back to the balancing forces of a single bubble (Fig. 1).

Depending on the predominant/prevailing bubble formation mechanism, some forces are negligible. The direction of the resistance force is a result of the liquid stream. In quiescent fluids the breakaway point of bubbles is later than in turbulent fluids. The bubble size can be calculated with equation 1. [1] (1)

$$\frac{d[(p]_g V_B v)}{dt} = F_{inertia} = F_{Resistance} = F_{Flotation} = F_{Pressure} = F_\sigma = F_{virtual\ Mass}$$

In the scrap melting chamber the conditions are turbulent because of the electromagnetic pumps (EMP) which are used to homogenize the melt temperature as well as the alloying element profile in the furnace and consequently for the increase of the melting rate. In this paper we will focus on the thermochemical modelling and the experimental proof of our results.

3 Thermochemical modelling

'FactSage' is used for the thermochemical modelling of the melting experiments to provide an overview of the possible reactions and their reaction products. It is taken into account in all the representations shown in this chapter that the calculations are always based on reaction equilibrium. The modelling software FactSage can access various materials databases (here Fact53, SGPS and SGTE). The equilibrium phases, which represent the system with the lowest total free enthalpy as a function of predetermined variables is based on Steady state conditions. The temperature is set to 750°C while the pressure of the melt and the added gas are set to 1 bar. The high metal volume used in the calculations has the consequence that the gases CO_2, CH_4 and CO are completely converted into solid reaction

products except for H_2.

In industrial scale the furnace atmosphere including the injected gas is constantly replaced and the remaining gaseous products are continuously removed from the reaction chamber. Accordingly the real system is an open one.

In Fig. 2 you see an example for a typical calculation done in this project. In this calculation one liter of AlMg3 alloy melt reacts with a variable amount of CO_2. The main products are MgO, Al_2O_3, Al_4C_3, $MgAl_2O_4$ and Al_2CO.

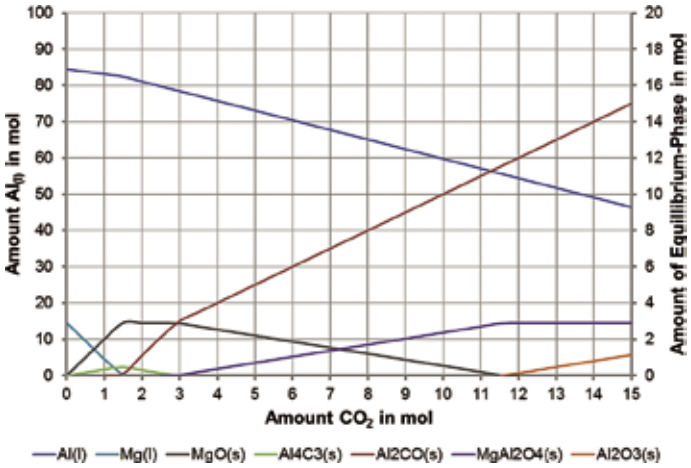

Fig. 2: Equilibrium phases for the reaction of 2350 g AlMg3 + <A> CO_2 with <A> up to 15 mol and under consideration of oxycarbide phases

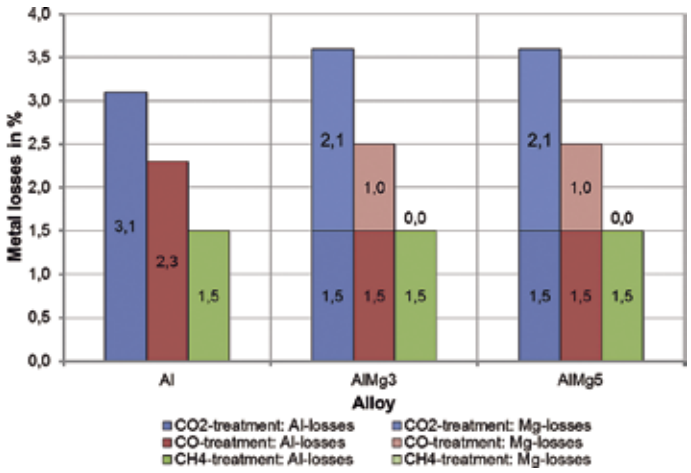

Fig. 3: Al and Mg losses in relation of Mg content and injected gas

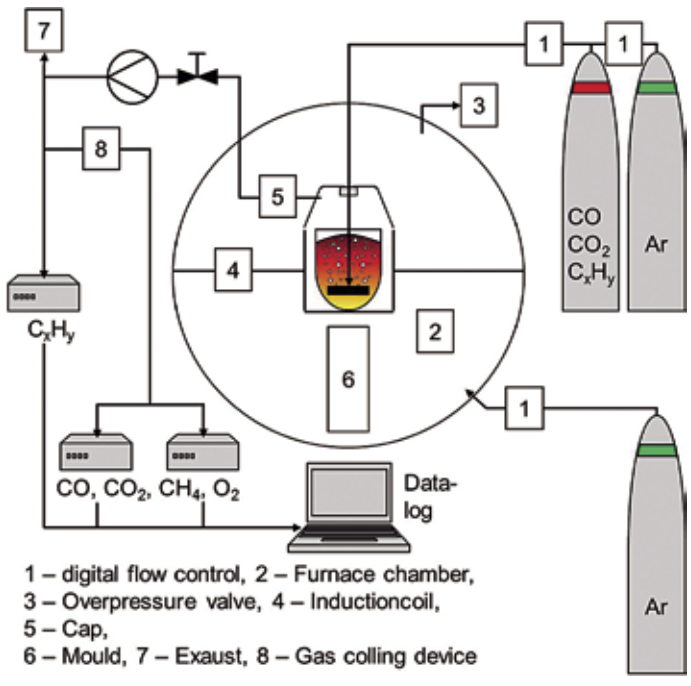

Fig. 4: Experimental setup with used gas analyzing system

It is easy to recognize that in the range up to 1.5 mol CO_2 magnesium is preferably oxidized from the alloy melt, while the carbon content of the gas is fully converted into Al_4C_3. Magnesium is no longer present in the melt at at an addition of 1.5 mol CO_2. At that point aluminum consumption increases. When the concentration of CO_2 reaches three mol, the balance shifts increasingly to the oxycarbide phase Al_2CO, while the amount of MgO phase remains constant. Above three moles of CO_2 there is no more aluminum carbide in the system. At the same point magnesium oxide is transformed into the spinel $MgAl_2O_4$, so that the amount of this equilibrium phase starts to increase. The magnesium oxide is completely transformed into the spinel at a CO_2 concentration of 11.5 mol. Alumina appears as an additional oxidation product of the reaction between aluminum and carbon dioxide as a result of the complete consumption of MgO.

In Fig. 3 the specific metal losses are presented in a bar chart diagram. The diagram shows the simulated aluminum and magnesium losses of the three investigated alloys. The results are grouped by the intended alloy and the gas species in different colours. The aluminum losses are shown in the lower bar part, while the magnesium losses of the AlMg alloys are added above in a weaker colour. The calculations revealed the metal losses for circa 87 mol aluminum or aluminum alloy (2,350 g) by addition of 1 mol of gas. The parameters have been pre-estimated to provide the opportunity to compare the calculated with the experimental results. As a consequence of this one mol of injected gas is used in the calculations, leading to a lack of oxygen in the system for full magnesium oxidation. As a result there is no observable difference between the AlMg3 and the AlMg5 alloy in the calculation.

4 Experiment

4.1 **Experimental setup:** For the experimental campaign of this work three different aluminum alloys AlMg3, AlMg5 and pure Al were used. The feeding material of all experiments has always the same size and surface in order to minimize a failure of different aluminum oxide amounts inherent to the charge materials. CO, CO_2 and CH_4 as typical de-coating products are injected into the melt. The following sketch (Fig. 4) shows the experimental setup.

All experiments are realized in an induction furnace. The used Al_2O_3 crucible has a volume of 1.3 litres. The induction coil is installed into a vacuum chamber which allows controlling the atmosphere inside the furnace. In all experiments the furnace atmosphere is 100% N_2. To realize a constant N_2 flow the gas is injected at the furnace bottom while the pressure is kept at 1 bar by an over pressure valve at the upper furnace. For injection of different gasses into the melt a glass lance is used. An exhaust hood above the crucible is used to collect the gaseous reaction products and the unconsumed gasses. An exhaust fan supplies the online quality gas measurement with the collected gasses. To make sure that no furnace atmosphere is sucked into the hood during the experiment more gas is injected than removed by the fan. Due to that the system has a slight over pressure under the hood, too.

Fig. 5a) shows a drawing of the gas injection system. The induction coil and the used hood to collect the gaseous products are shown in Fig. 5b).

In the first experimental campaign 12 tests are performed (Table 1). The gas injection time is limited by the crucible volume. The injection

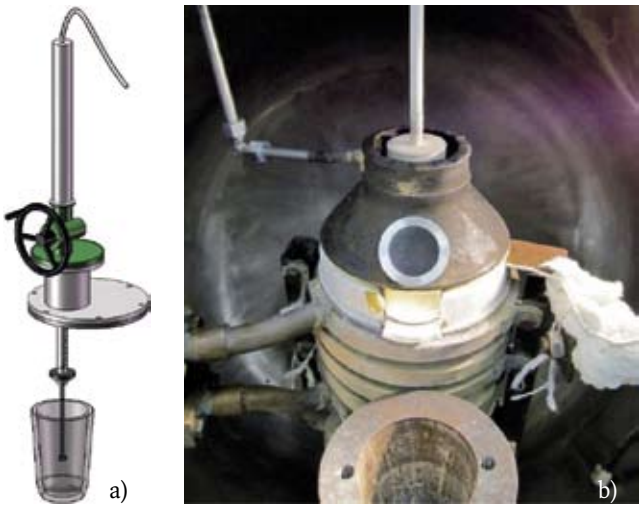

Fig. 5: a) Gas injection system; b) Induction coil with hood

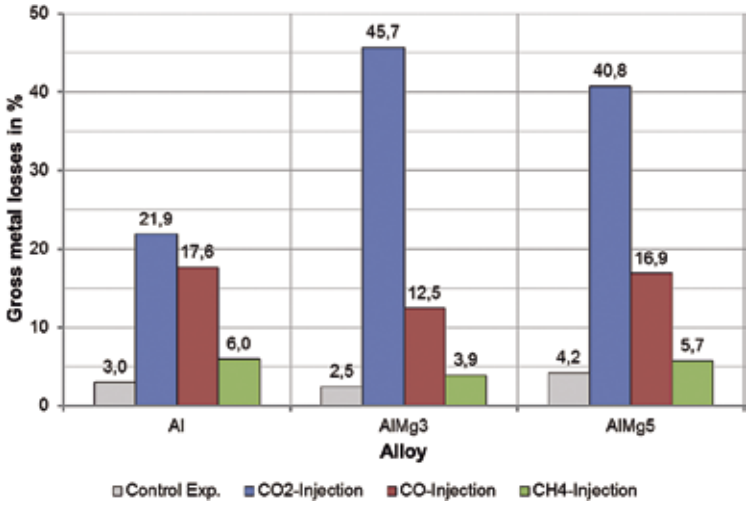

Fig. 6: Gross-remelting losses

of gas was stopped when the crucible is fully filled by dross. The gas composition is limited by the range of the installed gas analyzing system and also for security reasons.

4.2 Results

In Fig. 6 the metal losses of the tests are presented. They are grouped according to the used feedstock materials. The chart shows the gross-remelting losses, which are calculated by the ratio of final weight of the cast to initial weight of the feedstock, see equation 2.

$$remelting\ loss_{gross}\ in\ \% = \frac{m_{cast}}{m_{feedstock}} \qquad (2)$$

For the gross-remelting losses the metal content of the dross is not considered. The column chart compares the influence of different gases as well as the influence of the main alloying element (magnesium) on the gross-remelting losses.

The metal losses decrease for all three materials in the order of CO_2, CO and CH_4. The control experiments already indicated significant losses of the melt phase. In presence of magnesium the effect of carbon dioxide on the metal losses are doubled. The maximum loss of more than 45% is represent by the combination of the alloy AlMg3 and CO_2 as injected gas. A linear dependence on the magnesium content of the alloy to the gross metal loss is not evident.

To divide the metallic part from the non-metallic dross components a subsequent salt melt step is conducted. A typical salt flux (55% NaCl, 45% KCl and ≤ 1% CaF_2) is used. To guarantee a complete separation of metal and dross a high salt factor is adjusted.

The net-remelting losses of the melting experiments can be determined from the measured metal yields of the salt experiments, see equation 3: (3)

$$remelting\ loss_{net}\ in\ \% = \frac{m_{cast} + m_{recovered\ from\ dross}}{m_{feedstock}}$$

The results are shown in Fig. 7. The metal contents of the dross vary between 30 and 97% (average 70%). The net metal losses decrease in the same way like the gross metal losses according to the oxidation effect of the treatment gas, in the order of CO_2, CO and CH_4. The net-remelting losses of the control experiments increase from 0.1% via 0.4% through to 1.3% with rising magnesium content of the melt. In contrast to the gross metal losses the losses after metal separation by salt treatment rise for all three injected gases with increasing magnesium content. Thus, the metal loss values for CO and CH_4 treatment based on the three points show a linear dependence on magnesium concentration.

Comparing the gross and net metal losses it is good to see that the dross has a high metal content. This can be a result of dross handling and manual stripping but it can also be a result of the dross structure. It could be observed that especially in experiments with CO_2 injection the dross structure had a lot of layers each with metal film.

Before the dross is remelted under salt some samples are taken to analyze parts of the dross. The sampling is accomplished by optical criteria. XRD analyses have proven neither carbide nor oxycarbide phase while EDX analyses have shown the appropriate concentrations of Al, O and C, so that there is the possibility of an existing Aluminum-oxycarbide phase. Fig. 8 illustrates a typical SEM picture of one sample which is taken from the red marked area (see macroscopic photography on the upper right).

The average element level of the two red marked areas consists of 17,10 At.-% C, 18,70 At.-% O, 8,63 At.-% Mg and 55,58 At.-% Al (Fig. 8). The atomic components of aluminum and carbon are strongly represented. In contrast to the XRD analysis includes the EDX analysis the possibility of the presence of the carbide phase (Al_4C_3) and the oxycarbid phase (Al_2OC).

Experiment No.	Injected gas composition	Mg-Contentin Mass.-%	Treatment in min
NV1	N2 (Chamber atmosphere)	0	120
NV2	N2 (Chamber atmosphere)	2.82	20
NV3	N2 (Chamber atmosphere)	4.86	20
HV1KD	Ar + 15 Vol.-% CO_2	0	32
HV2KD	Ar + 15 Vol.-% CO_2	2.82	21
HV3KD	Ar + 15 Vol.-% CO_2	4.86	14
HV4KM	Ar + 7 Vol.-% CO	0	32
HV5KM	Ar + 7 Vol.-% CO	2.82	20
HV6KM	Ar + 7 Vol.-% CO	4.86	20
HV7KW	Ar + 5 Vol.-% CH_4	0	19
HV8KW	Ar + 5 Vol.-% CH_4	2.82	19
HV9KW	Ar + 5 Vol.-% CH_4	4.86	19

Table 1: Experimental plan

5 Conclusions

It should be underlined that all identified dependencies are related to the experimental

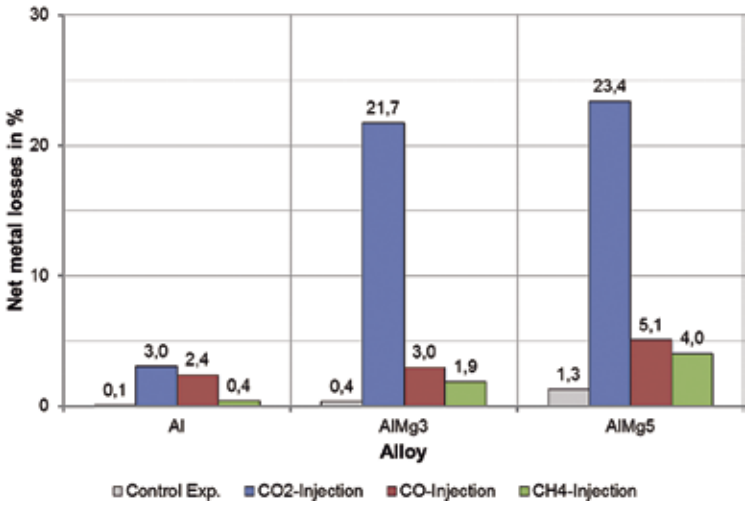

Fig. 7: Net-remelting losses

scale of one litre of melt. The behaviour of the reaction dynamics in a multiple chamber furnace can only carried out partially based on the performed experiments. The interactions of pyrolysis product gases and the aluminum melt and therefore the produced dross amount can diversify significantly through the increased scale and should therefore be tested in scale up trials.

The definition of the direct reaction products (mechanism) in accordance with the structural analysis is difficult, because on the one hand, a subsequent oxidation of possibly formed carbides and oxycarbides seems to be likely, and on the other hand, due to the high aluminum content in the taken samples the detection limit for minor components is quickly reached. Since carbide or oxycarbides in the considered region were not detected, it is unclear whether the result from FactSage issued for equilibrium phases are correct at all or if the phases are not present because of their post-oxidation under normal atmosphere. Since the thermochemical modelling of the melting experiments refers to the reaction equilibrium also a kinetic inhibition cannot be excluded.

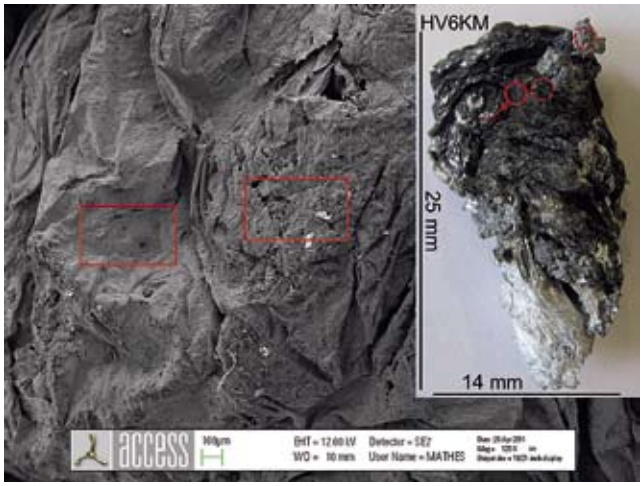

Fig. 8: SEM picture of the analyzed area (Experiment HV6KM)

The remelting losses decrease with decreasing oxygen content of the treatment gases, in the order from CO_2, CO, CH_4. By varying the feed material it has to be noted that the influence of each gas increases with increasing magnesium content of the melt. This trend is confirmed by the net metal losses, additionally approved by the online gas measurement.

Acknowledgement

The authors would like to thank the Hydro Aluminium Rolled Products GmbH for funding the studies, providing scrap materials for trails and also for their analytical support.

References

[1] Jaroni, B., Lucht, A., et al.: Conditions of Pyrolythic Processes in Multi Chamber Furnaces for Aluminium Recycling, Proceedings of European Metallurgical Conference EMC 2011

[2] Gnotke, O.: Experimentelle und theoretische Untersuchungen zur Bestimmung von veränderlichen Blasengrößen und Blasengrößenverteilungen in turbulenten Gas-Flüssgkeitsströmungen, Dissertation, Fachbereich Maschinenbau, TU Darmstadt, 2004

[3] von Röpenack, I.: Minimierung von Chlorgasemissionen bei der Spülgasraffination von Aluminiumschmelze, Dissertation, IME Aachen – Institut für Metallhüttenkunde und Elektrometallurgie, 1997

[4]Antrekowitsch, H. et al.: Spülgastechnik in der Kupferindustrie, in Berg- und Hüttenmännische Monatshefte, 149. Jahrgang, Heft Nr. 3, S.186-192, 2004